[redacted]

NACA RM L53D30

NACA

RESEARCH MEMORANDUM

CALCULATION OF AERODYNAMIC FORCES ON AN INCLINED DUAL-ROTATING PROPELLER

By John L. Crigler and Jean Gilman, Jr.

Langley Aeronautical Laboratory
Langley Field, Va.

NATIONAL ADVISORY COMMITTEE
FOR AERONAUTICS

WASHINGTON

June 19, 1953

[redacted]

NATIONAL ADVISORY COMMITTEE FOR AERONAUTICS

RESEARCH MEMORANDUM

CALCULATION OF AERODYNAMIC FORCES ON AN INCLINED DUAL-ROTATING PROPELLER

By John L. Crigler and Jean Gilman, Jr.

SUMMARY

A method is herein presented for calculating the aerodynamic forces on the blades of a dual-rotating propeller which has its thrust axis inclined to the air stream. This method makes use of Theodorsen's propeller theory for the calculation of the aerodynamic forces on the propeller blade. At any particular blade station and blade position the instantaneous flow field is presumed to be a steady-state condition for the whole propeller. Application of the method involves the use of two-dimensional airfoil characteristics as determined in a steady flow.

Calculations were made for an 8-blade NACA 8.75-(5)(05)-037 dual-rotating propeller operating at advance ratios of 1.20 and 3.25 for flight Mach numbers of 0.30 and 0.623, respectively. The thrust axis angle is 4° in both cases. Results of the calculations show that, in general, the fluctuations in aerodynamic forces on the front component are greater than the fluctuations in forces on the rear component. Comparisons with the forces on a single-rotating propeller show that the magnitude of the fluctuating forces on the front compone_ of a dual-rotating propeller is of the same order as the forces occurring on a single propeller operating at the same advance ratio, blade-angle setting, and inclination of the thrust axis.

Inasmuch as the front component of a dual-rotating propeller undergoes about the same variation in thrust coefficients as would a single-rotating propeller, the fact that smaller variations are encountered on the rear blades means that the one-cycle-per-revolution vibration problem for a pitched or yawed dual-rotating propeller is no more serious than for the single-rotating propeller.

INTRODUCTION

In reference 1 the magnitude of the aerodynamic forces on a single-rotating propeller in pitch or yaw was calculated under the assumption that the existing propeller theory may be used as though steady-state conditions existed successively at several angular positions of the propeller blade during one revolution. The method made use of the usual steady-state compressible-airfoil characteristics with Goldstein correction factors for a finite number of blades. The calculated results were compared with experimental data taken from a pitched propeller installation. The magnitude of the aerodynamic forces on the propeller blade calculated from the steady-state method was found to be in good agreement with the experimental data although there was some lag in the forces as shown by the experimental data. Further calculations based on the theory of oscillating airfoils in a pulsating flow (ref. 2) showed that the lag in air forces found in the experiments could be predicted.

The procedure followed for the case of the single-rotating propeller is inadequate in the dual case. In addition to the unsteady flow in the propeller plane caused by pitch or yaw, the effect of the flow field of each component on the other component for each position of the blade must be considered. In the case of the dual-rotating propeller the flow field of each component has been considered in making calculations of the forces on both components of a dual-rotating propeller in an effort to predict the magnitude of the differences in forces on the front and rear components. In view of the good agreement obtained in the case of the single-rotating propeller, it was assumed that steady-state conditions existed successively at the angular positions of the dual-rotating propeller during each revolution.

The oscillating air forces on the propeller blades cause vibratory stresses having a frequency of one per revolution. In this report the air forces are determined for each component of the dual-rotating propeller in an effort to determine the relative severity of the one-cycle-per-revolution vibration problem on the two components and to make a comparison with one component of the dual-rotating propeller when operating as a single propeller.

SYMBOLS

B	number of blades
b	chord of propeller-blade element, ft
c_d	section drag coefficient

[redacted]

c_l	section lift coefficient
c_{l_d}	design lift coefficient
C_T	thrust coefficient, $T/\rho n^2 D^4$
D	propeller diameter, ft
$\frac{dC_T}{dx}$	element thrust coefficient, $\frac{dT/dx}{\rho n^2 D^4}$
h	blade-section maximum thickness, ft
J	advance ratio, V/nD
K(x)	circulation function
M	Mach number of advance
n	propeller rotational speed, rps
R	tip radius, ft
r	radius to any blade element, ft
T	thrust, lb
t	time, sec
V	velocity of advance, ft/sec
W	resultant velocity at blade section, ft/sec
W_o	geometric resultant velocity, ft/sec
w	rearward displacement velocity of helical vortex sheet
$\overline{w}$	velocity ratio $w/V \cos \alpha_T$
x	radial location of blade element, r/R
α	angle of attack, deg
α_T	angle of inclination of propeller thrust axis, deg
β	blade angle, deg

[redacted]

$\gamma = \tan^{-1} \frac{c_d}{c_l}$

κ mass-flow coefficient, $2 \int_0^1 K(x)x \, dx$

ρ mass density of air, slugs/cu ft

σ solidity, $Bb/2\pi r$

σc_l propeller-element load coefficient

ϕ aerodynamic helix angle, deg

ϕ_o geometric helix angle, deg

ω angular velocity of propeller, $2\pi n$, radians/sec

Subscripts:

F front

R rear

S front component of a dual-rotating propeller operating as a single-rotating propeller

ωt denotes angular position of blade required to give instantaneous values, deg

AERODYNAMICS OF THE INCLINED PROPELLER

The Velocity Diagram

The velocity diagram for a blade section of a single-rotating inclined propeller is discussed in reference 1. This diagram is reproduced herein as figure 1. The convention adopted in reference 1 was to consider the time variable ωt, which defines the angular position of the blade, to be zero when the blade is initially vertically upward with the propeller axis in positive pitch and measured in the direction of rotation (the axes used in defining the blade position may be rotated to comply with propeller attitudes other than pitch).

From figure 1, the geometric helix angle is given by

$$\left(\phi_o\right)_{\omega t} = \tan^{-1} \frac{V \cos \alpha_T}{\pi n D x + V \sin \alpha_T \sin \omega t}$$

or

$$\left(\phi_o\right)_{\omega t} = \tan^{-1} \frac{\cos \alpha_T}{\frac{\pi x}{J} + \sin \alpha_T \sin \omega t} \tag{1}$$

The resultant velocity is given by

$$\left(W_o\right)_{\omega t} = \sqrt{V^2 \cos^2 \alpha_T + \left(\pi n D x + V \sin \alpha_T \sin \omega t\right)^2} \tag{2}$$

The local advance ratio is given by

$$J_{\omega t} = \frac{\pi x \cos \alpha_T}{\frac{\pi x}{J} + \sin \alpha_T \sin \omega t} \tag{3}$$

From equation (3) the local advance ratio is seen to vary, the amount of variation depending on the position of the blade. In making steady-state calculations of the forces and moments on the blade of a single-rotating pitched propeller in reference 1, a change in blade position was treated as a change in operating V/nD in accordance with equation (3). For the single-rotating propeller the solution is adequate when the calculations are based on the local geometric helix angle inasmuch as complete calculations were made as though the entire propeller operated successively at the different blade positions and the induced effects were incorporated in each calculation.

The velocity diagram for the blade sections of a dual-rotating propeller showing the effect of the induced flow of each component on the other component is given in figure 2. This diagram is reproduced from reference 3.

For inclined dual-rotating propellers the alteration to the geometric velocity field due to oscillating velocities for the front propeller unit

[redacted]

is similar to the alteration for single-rotating propellers, that is,

$$\tan\left(\phi_{o_{\omega t}}\right)_F = \frac{V \cos \alpha_T}{\pi n D x + V \sin \alpha_T \sin \omega t}$$

$$= \frac{\cos \alpha_T}{\frac{\pi x}{J} + \sin \alpha_T \sin \omega t} \tag{4}$$

The rear propeller is of opposite rotation and, in order to make use of the same reference axes for measuring the blade-position angle as is used for the front propeller, it is convenient to write

$$\tan\left(\phi_{o_{\omega t}}\right)_R = \frac{V \cos \alpha_T}{\pi n D x - V \sin \alpha_T \sin \omega t}$$

$$= \frac{\cos \alpha_T}{\frac{\pi x}{J} - \sin \alpha_T \sin \omega t} \tag{5}$$

This reversal of sign for the front- and rear-propeller units is used throughout the development of the equations for the aerodynamic helix angles and element loading coefficients.

In addition to the alteration to the geometric velocity field for the dual-rotating propeller, it is necessary to consider the influence of the velocity field of each component of the propeller on the other component before performance calculations can be made. Theodorsen's propeller theory was used to determine the flow field of each component due to the other component. Admittedly, this method has the defect that it was developed for the idealized case in which the two components have the same load distribution and equal power absorption. However, if it is assumed that the mass-flow coefficient and the circulation functions for a given number of blades apply for nonoptimum distribution, the method with these assumptions gives a close approximation to the flow field since both of these functions are primarily dependent on the geometric helix angle and show only small variations with loading for a given geometric helix angle and blade number. This dual-rotating-propeller case is analogous to the use of Goldstein functions for the several blade

positions in the case of single-rotating propellers as developed in reference 1. The interference velocities for the dual-rotating propeller and the effect of each component on the flow field of the other component are shown in reference 3. Since the front and rear components of the dual-rotating propeller are unequally loaded for each phase angle and the loading changes with a change in phase angle, it is necessary to make successive approximations to the mass-flow coefficient κ and to the displacement velocity w for each phase angle calculated.

Method of Calculation

The resultant velocity, the aerodynamic helix angle, and the element loading coefficient for a radial station of an optimum dual-rotating propeller are given in reference 3 as

$$W_F = \frac{V}{\sin \phi_o}\left(1 + \frac{1}{4}\kappa\bar{w} \sin^2\phi_o\right) \tag{6}$$

$$W_R = \frac{V}{\sin \phi_o}\left(1 + \frac{3}{4}\kappa\bar{w} \sin^2\phi_o\right) \tag{7}$$

$$\tan \phi_F = \frac{J}{\pi x}\left[1 + \frac{1}{2}\bar{w}\left(1 + \frac{1}{2}\kappa \tan^2\phi\right)\right] \tag{8}$$

$$\tan \phi_R = \frac{J}{\pi x}\left[1 + \frac{1}{2}\bar{w}\left(1 - \frac{1}{2}\kappa \tan^2\phi\right)\right] \tag{9}$$

$$\left(\sigma c_l\right)_F = \frac{J}{\pi x}\frac{(1 + \bar{w})\bar{w} \sin \phi_o K(x)}{1 + \frac{1}{4}\kappa\bar{w} \sin^2\phi_o} \tag{10}$$

$$\left(\sigma c_l\right)_R = \frac{J}{\pi x}\frac{(1 + \bar{w})\bar{w} \sin \phi_o K(x)}{1 + \frac{3}{4}\kappa\bar{w} \sin^2\phi_o} \tag{11}$$

[redacted]

where

$$\tan \phi = \frac{J}{\pi x}\left(1 + \frac{1}{2}\overline{w}\right) \tag{12}$$

A method of applying Theodorsen's propeller theory to the calculation of the aerodynamic forces on the propeller blade for nonideal dual-rotating propellers is described in reference 4. The method essentially consists of solving for local values of $\overline{w}$ along the blade by a method of cross-plotting by using equations (8) to (12).

The method, as developed in reference 4, has been found to be satisfactory when the loading on the two components of the propeller is close to the same but should not be used when the difference in loading becomes large. Consequently, the changes developed in the present report have been incorporated in the addenda to reference 4. The method, as developed herein, shows good agreement with experimental data even for large differences in loadings on the two components of the propeller as shown in the addenda of reference 4.

For inclined dual-rotating propellers the propeller-performance equations require modification to account for the oscillating velocities. The resultant velocity, the aerodynamic helix angle, and the element loading as modified are given to a first approximation for the front components by

$$(W_{\omega t})_F = \frac{V \cos \alpha_T}{\sin \phi_{o_{\omega t}}}\left(1 + \frac{1}{4}\kappa_{\omega t}\overline{w}_{\omega t} \sin^2\phi_{o_{\omega t}}\right) \tag{13}$$

$$\left(\phi_o\right)_{\omega t_F} = \tan^{-1}\frac{V \cos \alpha_T}{\pi n D x + V \sin \alpha_T \sin \omega t} \tag{14}$$

$$\tan\left(\phi_{\omega t}\right)_F = \frac{\cos \alpha_T\left[1 + \frac{1}{2}\overline{w}_{\omega t}\left(1 + \frac{1}{2}\kappa_{\omega t} \tan^2\phi_{\omega t}\right)\right]}{\frac{\pi x}{J} + \sin \alpha_T \sin \omega t} \tag{15}$$

[redacted]

where

$$\left.\begin{aligned} \overline{w}_{\omega t} &= \frac{w_{\omega t}}{V \cos \alpha_T} \\ \tan \phi_{\omega t} &= \frac{V \cos \alpha_T \left(1 + \frac{1}{2} \overline{w}_{\omega t}\right)}{\pi n D x + V \sin \alpha_T \sin \omega t} \end{aligned}\right\} \tag{16}$$

The effect of the inclined thrust axis on a dual-rotating propeller is seen to be the same as rotating the two components at unequal speeds. Equations for the rear component are obtained by a similar modification.

In calculating propeller characteristics by Theodorsen's theory as applied in reference 3 the average axial interference velocity κw was assumed to be equally due to each of the two components. When the loading is not the same on the front and rear components, or effectively, the rotational speeds are unequal, as in the present case, the interference velocity will not be equally due to each component and may be looked upon as broken into two unequal parts $(\kappa w)_F$ and $(\kappa w)_R$ where the average axial interference velocity in the final wake is $\kappa w = \frac{(\kappa w)_F + (\kappa w)_R}{2}$ but $(\kappa w)_F \neq (\kappa w)_R$. The expression $(\kappa w)_F$ refers to the interference velocity that would be obtained in the final wake if the loading on the rear component were equal to the loading on the front component of a dual-rotating propeller. Similarly, $(\kappa w)_R$ refers to the interference velocity that would be obtained if the loading on the front component were equal to the loading on the rear component of a dual-rotating propeller. Thus, when the two components are equally loaded and of opposite rotation, the interference velocity is equally due to each component and $\kappa w = (\kappa w)_F = (\kappa w)_R$.

In the solution the interference velocity associated with each component will result in different values of $\phi_{\omega t}$ for the two components of the propeller. The values of w_F and w_R are first calculated separately just as though each component operates in the presence of another component equally and oppositely loaded. The method is equivalent to assuming that ideal functions apply to nonoptimum loadings and ideal values of κ and $K(x)$ are used. This practice has been generally successful in single-rotating propellers where Goldstein's tip correction factors are used for nonoptimum loadings. In the solution it is adequate to replace ϕ by ϕ_{o_F} or ϕ_{o_R} in the induced velocities. Equations (13) and (15) as modified now become

[redacted]

$$W_{\omega t_F} = \frac{V \cos \alpha_T}{\sin(\phi_o)_{\omega t_F}} \left\{ 1 + \frac{1}{4} \left[\frac{(\kappa \bar{w})_{\omega t_F} + (\kappa \bar{w})_{\omega t_R}}{2} \right] \sin^2(\phi_o)_{\omega t_F} \right\} \tag{17}$$

$$\tan(\phi)_{\omega t_F} = \frac{\cos \alpha_T \left[1 + \frac{1}{2} \bar{w}_{\omega t_F} + \frac{1}{4} (\kappa \bar{w})_{\omega t_F} \tan^2(\phi)_{\omega t_1} \right]}{\frac{\pi x}{J} + \sin \alpha_T \sin \omega t} \tag{18}$$

where

$$\tan(\phi)_{\omega t_1} = \frac{\cos \alpha_T \left(1 + \frac{1}{2} \bar{w}_{\omega t_F} \right)}{\frac{\pi x}{J} + \sin \alpha_T \sin \omega t} \tag{19}$$

Similarly, for the rear propeller with due regard to the reversal in sign because of opposite rotation in obtaining the aerodynamic helix angle,

$$W_{\omega t_R} = \frac{V \cos \alpha_T}{\sin(\phi_o)_{\omega t_R}} \left[1 + \frac{1}{4} \frac{(\kappa \bar{w})_{\omega t_F} + (\kappa \bar{w})_{\omega t_R}}{2} \sin^2(\phi_o)_{\omega t_R} + \frac{1}{2} (\kappa \bar{w})_{\omega t_F} \sin^2(\phi_o)_{\omega t_R} \right]$$

or

$$W_{\omega t_R} = \frac{V \cos \alpha_T}{\sin(\phi_o)_{\omega t_R}} \left\{ 1 + \frac{1}{2} \sin^2(\phi_o)_{\omega t_R} \left[\frac{5}{4} (\kappa \bar{w})_{\omega t_F} + \frac{1}{4} (\kappa \bar{w})_{\omega t_R} \right] \right\} \tag{20}$$

[redacted]

and

$$\tan(\phi)_{\omega t_R} = \frac{\cos \alpha_T \left[1 + \frac{1}{2} \bar{w}_{\omega t_R} - \frac{1}{2}(\kappa \bar{w})_{\omega t_F} \tan^2 \phi_{\omega t_1} + \frac{1}{4}(\kappa \bar{w})_{\omega t_R} \tan^2 \phi_{\omega t_2}\right]}{\frac{\pi x}{J} - \sin \alpha_T \sin \omega t} \tag{21}$$

where

$$\tan \phi_{\omega t_2} = \frac{\cos \alpha_T \left(1 + \frac{1}{2} \bar{w}_{\omega t_R}\right)}{\frac{\pi x}{J} - \sin \alpha_T \sin \omega t} \tag{22}$$

It can be seen that, for equal loadings on the front and rear components where $(\kappa w)_F = (\kappa w)_R$, equations (17), (18), (20), and (21) reduce to the same form as in reference 3.

The element loading coefficient as modified for the inclined dual-rotating propeller is

$$\sigma c_{l_{\omega t_F}} = \frac{\cos \alpha_T \left[\left(1 + \bar{w}_{\omega t_F}\right) \bar{w}_{\omega t_F} \sin(\phi_o)_{\omega t_F} K(x)_{\omega t_F}\right]}{\left(\frac{\pi x}{J} + \sin \alpha_T \sin \omega t\right)\left[1 + \frac{1}{4}\left(\frac{\kappa \bar{w}_{\omega t_F} + \kappa \bar{w}_{\omega t_R}}{2}\right) \sin^2(\phi_o)_{\omega t_F}\right]} \tag{23}$$

where $\left[K(x)_{\omega t}\right]_F$ is based on $\frac{V + w}{nD} = \pi x \tan(\phi_o)_{\omega t_F}\left(1 + \bar{w}_{\omega t_F}\right)$ for the front component and

$$(\sigma c_l)_{\omega t_R} = \frac{\cos \alpha_T \left(1 + \bar{w}_{\omega t_R}\right) \bar{w}_{\omega t_R} \sin(\phi_o)_{\omega t_R} K(x)_{\omega t_R}}{\left(\frac{\pi x}{J} - \sin \alpha_T \sin \omega t\right)\left\{1 + \frac{1}{2} \sin^2 \phi_{o\ \omega t_R}\left[\frac{5}{4}(\kappa \bar{w})_{\omega t_F} + \frac{1}{4}(\kappa \bar{w})_{\omega t_R}\right]\right\}} \tag{24}$$

where $\left[K(x)_{\omega t}\right]_R$ is based on $\pi x \tan(\phi_o)_{\omega t_R}\left(1 + \bar{w}_{\omega t_R}\right)$ for the rear component. Finally, the thrust equation is given by

[redacted]

$$dT = \frac{1}{2}\rho W^2 Bb(c_l \cos \phi - c_d \sin \phi)dr \tag{25}$$

By definition,

$$x = \frac{r}{R} = \frac{2r}{D}$$

$$dx = \frac{2dr}{D}$$

$$\sigma = \frac{Bb}{2\pi r}$$

$$\tan \gamma = \frac{c_d}{c_l}$$

therefore, equation (25) may be reduced to

$$\frac{dT}{dx} = \frac{\pi D^2}{4} x\rho W^2 \sigma c_l \cos \phi(1 - \tan \gamma \tan \phi) \tag{26}$$

By substituting the value of W from equation (17) and replacing ϕ by the value of $\phi_{\omega t_F}$ and dividing both sides by $\rho n^2 D^4$ the thrust equation for the front component in coefficient form is reduced to

$$\left(\frac{dC_T}{dx}\right)_{\omega t_F} = \frac{\pi x}{4} \frac{J^2 \cos^2 \alpha_T}{\sin^2(\phi_o)_{\omega t_F}} \left\{1 + \frac{1}{4}\left[\frac{(\kappa\bar{w})_{\omega t_F} + (\kappa\bar{w})_{\omega t_R}}{2}\right] \sin^2(\phi_o)_{\omega t_F}\right\}^2$$

$$(\sigma c_l)_{\omega t_F} \cos(\phi)_{\omega t_F} \left[1 - \tan(\phi)_{\omega t_F} \tan \gamma_{\omega t_F}\right] \tag{27}$$

[redacted]

Similarly, for the rear component

$$\left(\frac{dC_T}{dx}\right)_{\omega t_R} = \frac{\pi x}{4} \frac{J^2 \cos^2 \alpha_T}{\sin^2(\phi_o)_{\omega t_R}} \left\{ 1 + \frac{1}{2} \sin^2(\phi_o)_{\omega t_R} \left[\frac{5}{4} (\kappa \bar{w})_{\omega t_F} + \frac{1}{4} (\kappa \bar{w})_{\omega t_R} \right] \right\}^2$$

$$(\sigma c_l)_{\omega t_R} \cos(\phi)_{\omega t_R} \left[1 - \tan(\phi)_{\omega t_R} \tan \gamma_{\omega t_R} \right] \qquad (28)$$

RESULTS OF SAMPLE CALCULATIONS

Calculations of the elemental-thrust variations have been made for an 8.75-foot-diameter 8-blade dual-rotating propeller having an NACA 8.75-(5)(05)-037 blade design. Blade-form curves for this propeller are given in figure 3. NACA 16-series airfoil data appropriate to the various section Mach numbers encountered in making the calculations were interpolated from reference 5.

In order to include the effect of advance ratio on the fluctuating-forces calculations were made for both a low advance ratio ($J = 1.2$) and for a relatively high advance ratio ($J = 3.25$). The thrust axis angle α_T was maintained constant at 4°. This angle was selected as being large enough to show significant effects of inclination on the fluctuating forces but not so large as to create blade-section angles of attack in the stalled range where airfoil data are usually unavailable for making the calculations. For the low-speed case ($J = 1.2$) the flight Mach number is 0.30. The blade-angle settings are $\beta_{F_{0.7R}} = 32.41^\circ$ and $\beta_{R_{0.7R}} = 31.53^\circ$. For the high-speed case ($J = 3.25$), the flight Mach number is 0.623. The blade-angle settings are $\beta_{F_{0.7R}} = 57.69^\circ$ and $\beta_{R_{0.7R}} = 56.15^\circ$. In either case the blade-angle settings used would give equal power absorption on the front and rear components with $\alpha_T = 0^\circ$. Figures 4 and 5 show typical results for several radial stations investigated for $J = 1.2$ and $J = 3.25$, respectively. Instantaneous values of $C_{T_{\omega t_{F,R}}}$ as a function of ωt are shown in figures 6 and 7 for $J = 1.2$ and $J = 3.25$, respectively. The elemental-thrust coefficients

[redacted]

for the front component of the dual-rotating propeller operating as a single-rotating propeller at the same J, α_T, and $\beta_{0.7R}$ were calculated by the method given in reference 1 for one condition in order to give a comparison of the difference in forces on a single- and dual-rotating propeller. These results (for $J = 3.25$) are included in figure 5 and the integrated values showing the variation of the instantaneous thrust coefficient $C_{T_{\omega t}}$ are shown in figure 7.

Both the elemental-thrust coefficients for the various radial stations plotted as a function of angular blade position (figs. 4 and 5) and the integrated thrust (figs. 6 and 7) show that the difference between the maximum and minimum forces, shown by the fluctuations in thrust coefficients, is greater on the front component than on the rear component of a dual propeller. The fluctuations in thrust coefficients on the front component of a dual propeller, due to pitched operation, differ only slightly from the fluctuations in thrust coefficients on a single-rotating propeller operating at the same J, α_T, and blade-angle setting. The value of $\left(C_{T_{\omega t=90^\circ}} - C_{T_{\omega t=270^\circ}}\right)_F$ for the low-speed case ($J = 1.2$, fig. 6) is 0.0420 for the front propeller and is 13 percent higher than the value of $\left(C_{T_{\omega t=270^\circ}} - C_{T_{\omega t=90^\circ}}\right)_R$ of 0.0373 for the rear propeller. A similar comparison for the high-speed case ($J = 3.25$, fig. 7) gives a value of $\left(C_{T_{\omega t=90^\circ}} - C_{T_{\omega t=270^\circ}}\right)_F$ of 0.216 which is 28 percent higher than the value of $\left(C_{T_{\omega t=270^\circ}} - C_{T_{\omega t=90^\circ}}\right)_R$ of 0.168 for the rear propeller. The comparison of the fluctuation in forces of the front component of the dual-rotating propeller with the single-rotating propeller would be expected to show about the same variations since the velocity field of the front component is affected by the average axial-interference velocity only of the rear component which is, in general, rather small. The rear component is affected by the axial- and rotational-interference velocities of the front component, but the rotational-interference velocity tends to decrease the magnitude of the fluctuating forces on the rear component compared with the front component. Inasmuch as the rotational interference velocities increase with an increase in operating J, the fluctuating forces on the rear component decrease compared with the forces on the front component.

This discussion is only intended to apply to the oscillating air forces on the blades that cause vibratory stresses having a frequency of one per revolution. Other effects such as blade passage and effects of blade structure are not within the scope of this paper.

[redacted]

SUMMARY OF RESULTS

A method is herein presented for calculating the fluctuating aerodynamic forces on pitched or yawed dual-rotating propellers. Typical examples have indicated the following results:

1. Comparison of the fluctuating aerodynamic forces due to pitched or yawed operation of a dual-rotating propeller show that, in general, the fluctuation in forces on the front component are greater than the fluctuation in forces on the rear component.

2. The differences in the magnitude of the fluctuating forces increase as the operating advance ratio is increased.

3. The magnitude of the fluctuating forces on the front component of a dual-rotating propeller are of the same order as the forces occurring on a single-rotating propeller operating at the same advance ratio, blade-angle setting, and inclination of the thrust axis.

4. The one-cycle-per-revolution vibration problem for the dual-rotating propeller is no more serious than for the single-rotating propeller when operating at the same advance ratio, blade-angle setting, and inclination of the thrust axis.

Langley Aeronautical Laboratory,
National Advisory Committee for Aeronautics,
Langley Field, Va.

[redacted]

REFERENCES

1. Crigler, John L., and Gilman, Jean, Jr.: Calculation of Aerodynamic Forces on a Propeller in Pitch or Yaw. NACA TN 2585, 1952.

2. Greenberg, J. Mayo: Airfoil in Sinusoidal Motion in a Pulsating Stream. NACA TN 1326, 1947.

3. Crigler, John L.: Application of Theodorsen's Theory to Propeller Design. NACA Rep. 924, 1949. (Supersedes NACA RM L8F30.)

4. Gilman, Jean, Jr.: Application of Theodorsen's Propeller Theory to the Calculation of the Performance of Dual-Rotating Propellers. NACA RM L51A17, 1951. (With Errata and Addenda No. 1, 1953.)

5. Enos, L. H., and Borst, H. V.: Propeller Performance Analysis. Aerodynamic Characteristics, NACA 16 Series Airfoils. Pt. II. Rep. No. C-2000, Curtiss-Wright Corp., Propeller Div. (Caldwell, N.J.), Dec. 2, 1948.

[redacted]

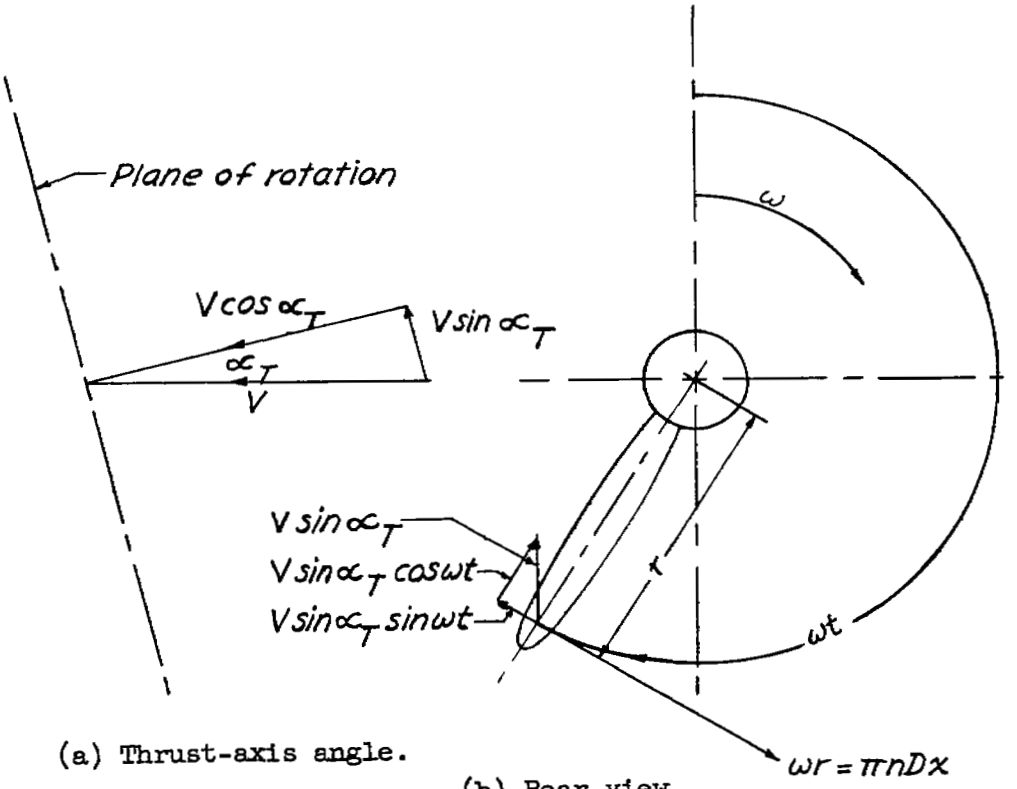

(a) Thrust-axis angle.

(b) Rear view.

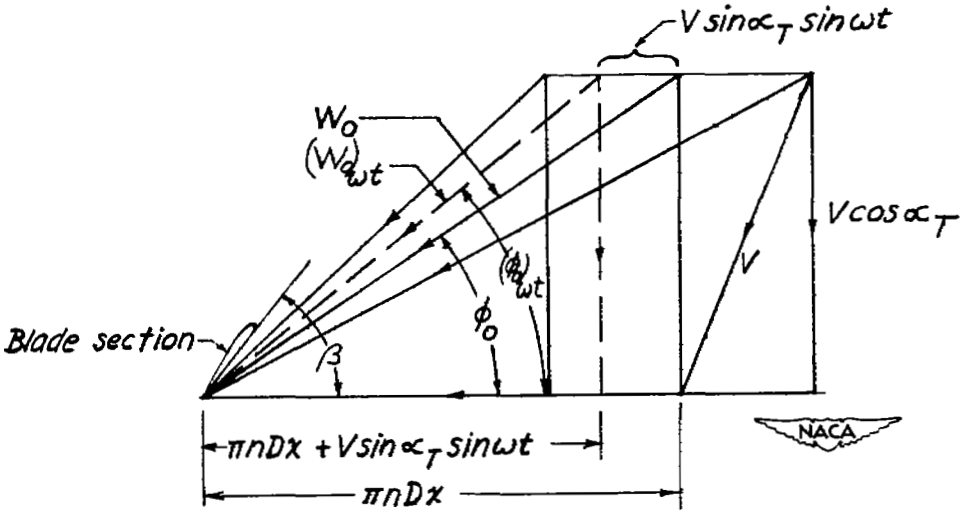

(c) Velocity vectors.

Figure 1.- Velocity diagram of inclined propeller (from ref. 1).

[redacted]

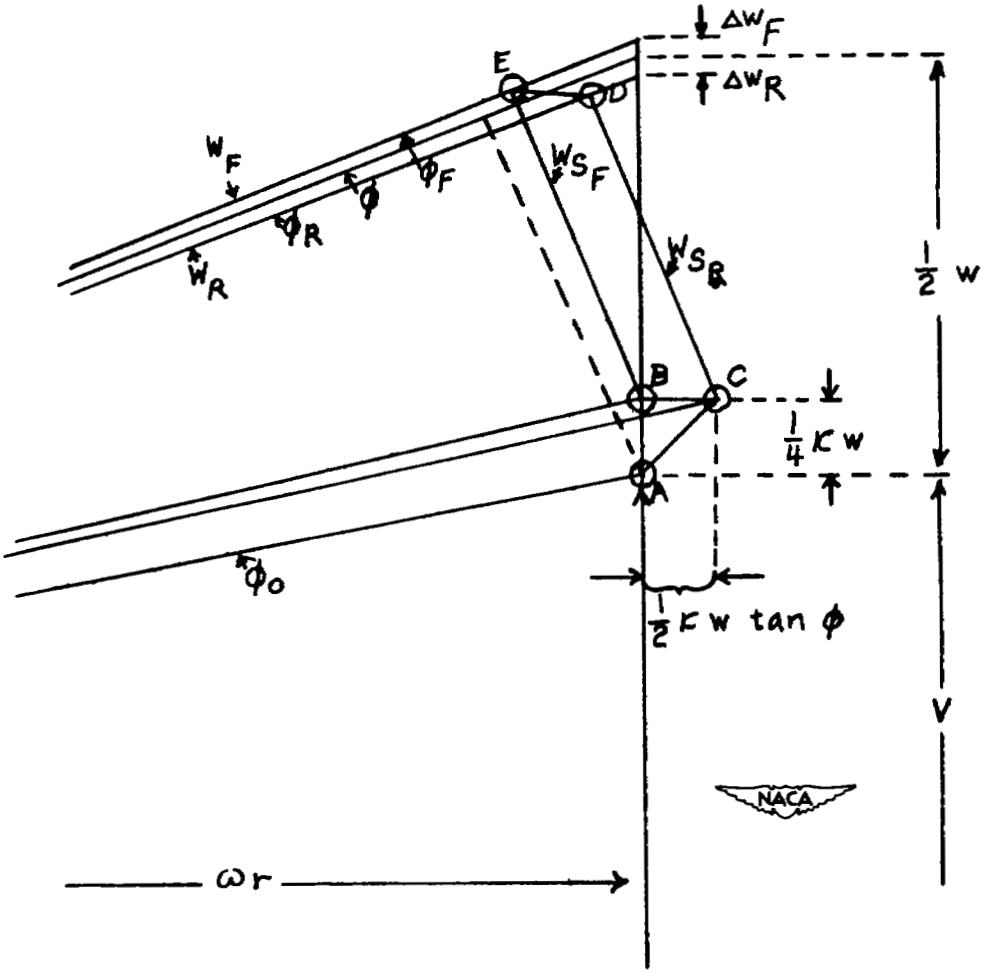

Figure 2.- Velocity diagram for dual-rotating propeller (from ref. 3).

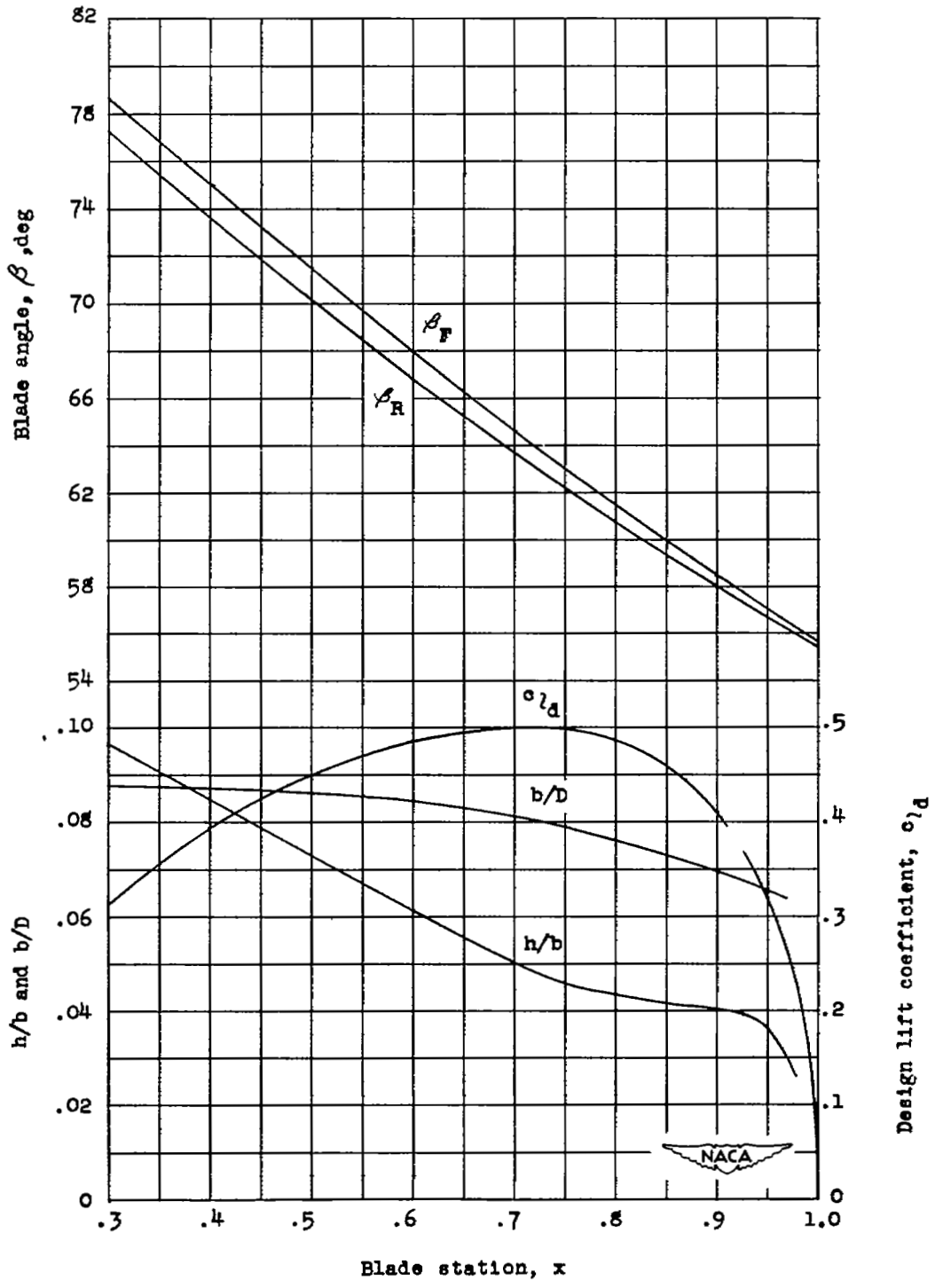

Figure 3.- Blade-form curves and pitch distribution of NACA 8.75-(5)(05)-037 dual-rotating propeller.

[redacted]

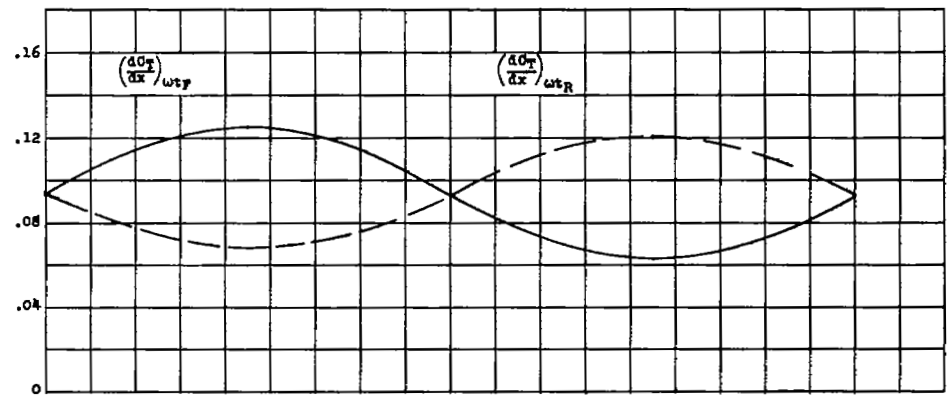

(a) $x = 0.5$.

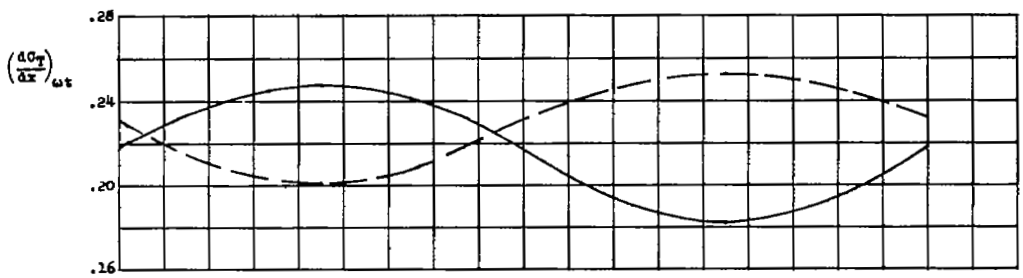

(b) $x = 0.7$.

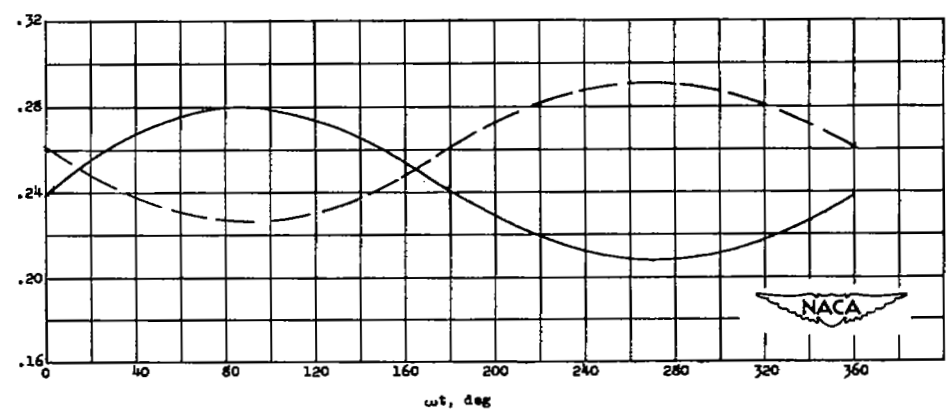

(c) $x = 0.9$.

Figure 4.- Typical results of calculations showing $\left(\frac{dC_T}{dx}\right)_{\omega t_{F,R}}$ as a function of ωt for several radii of the NACA 8.75-(5)(05)-037 propeller. $M = 0.30$; $J = 1.2$; $\alpha_T = 4^\circ$.

[redacted]

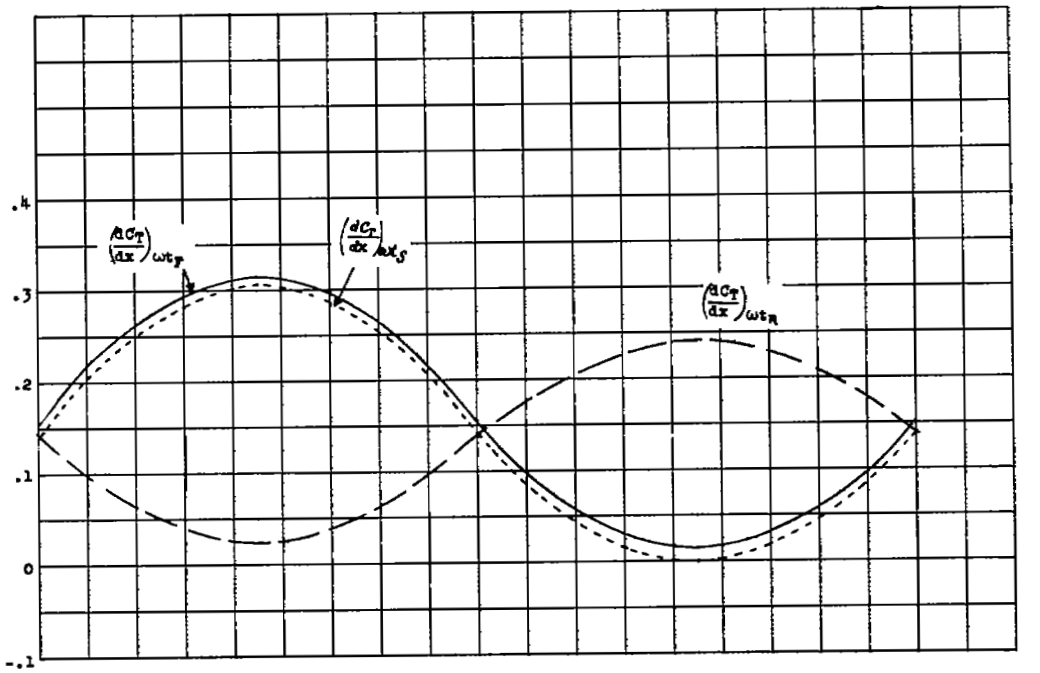

(a) x = 0.5.

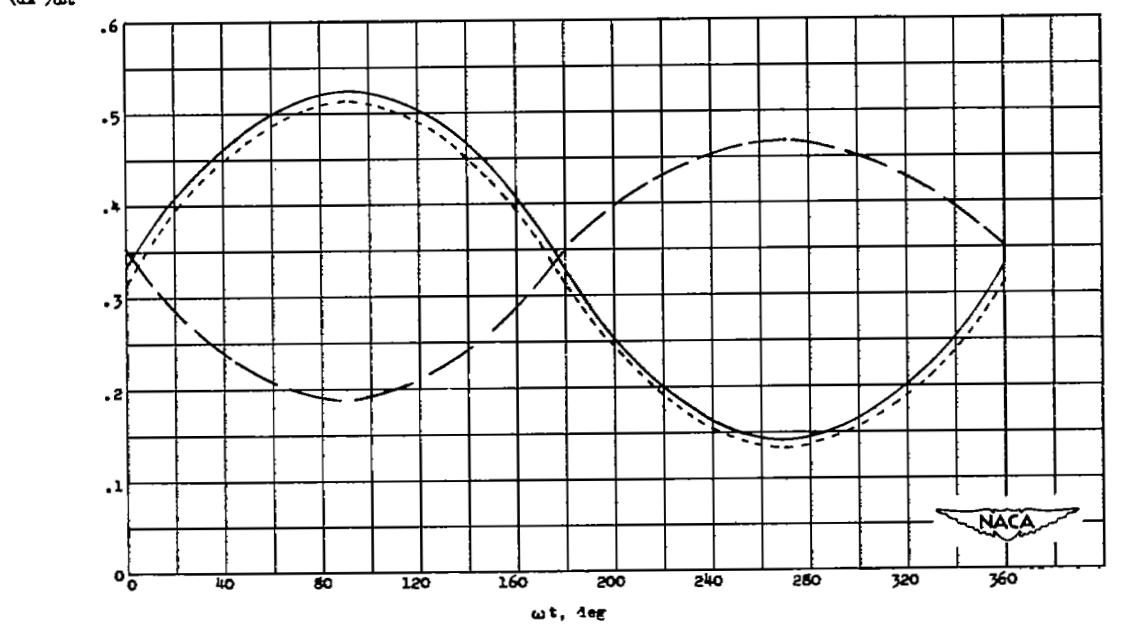

(b) x = 0.7.

Figure 5.- Typical results of calculations showing $\left(\frac{dC_T}{dx}\right)_{\omega t_{F,R}}$ as a function of ωt for several radii on the NACA 8.75-(5)(05)-037 propeller. M = 0.623; J = 3.25; $\alpha_T = 4^\circ$.

[redacted]

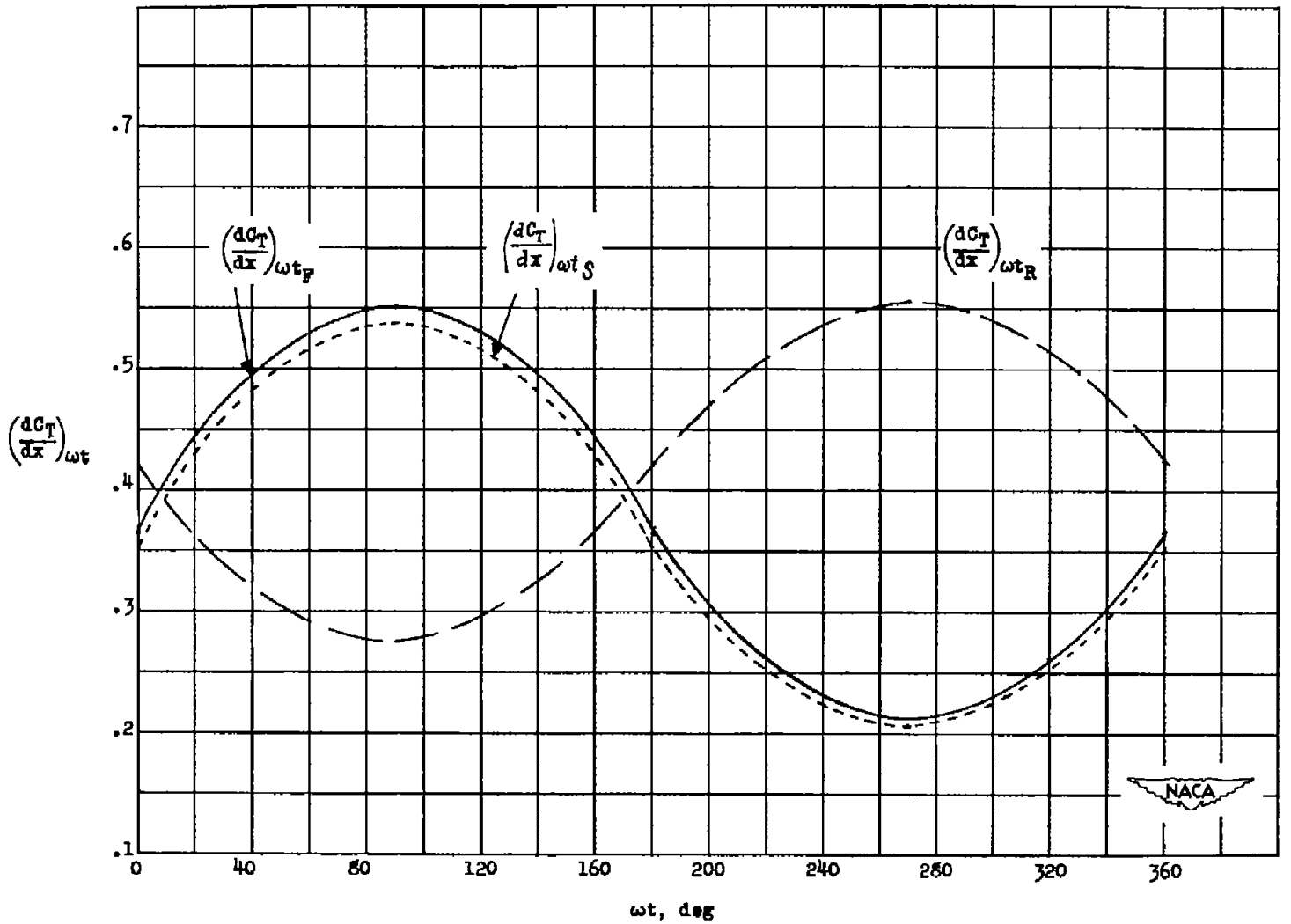

(c) x = 0.9.

Figure 5.- Concluded.

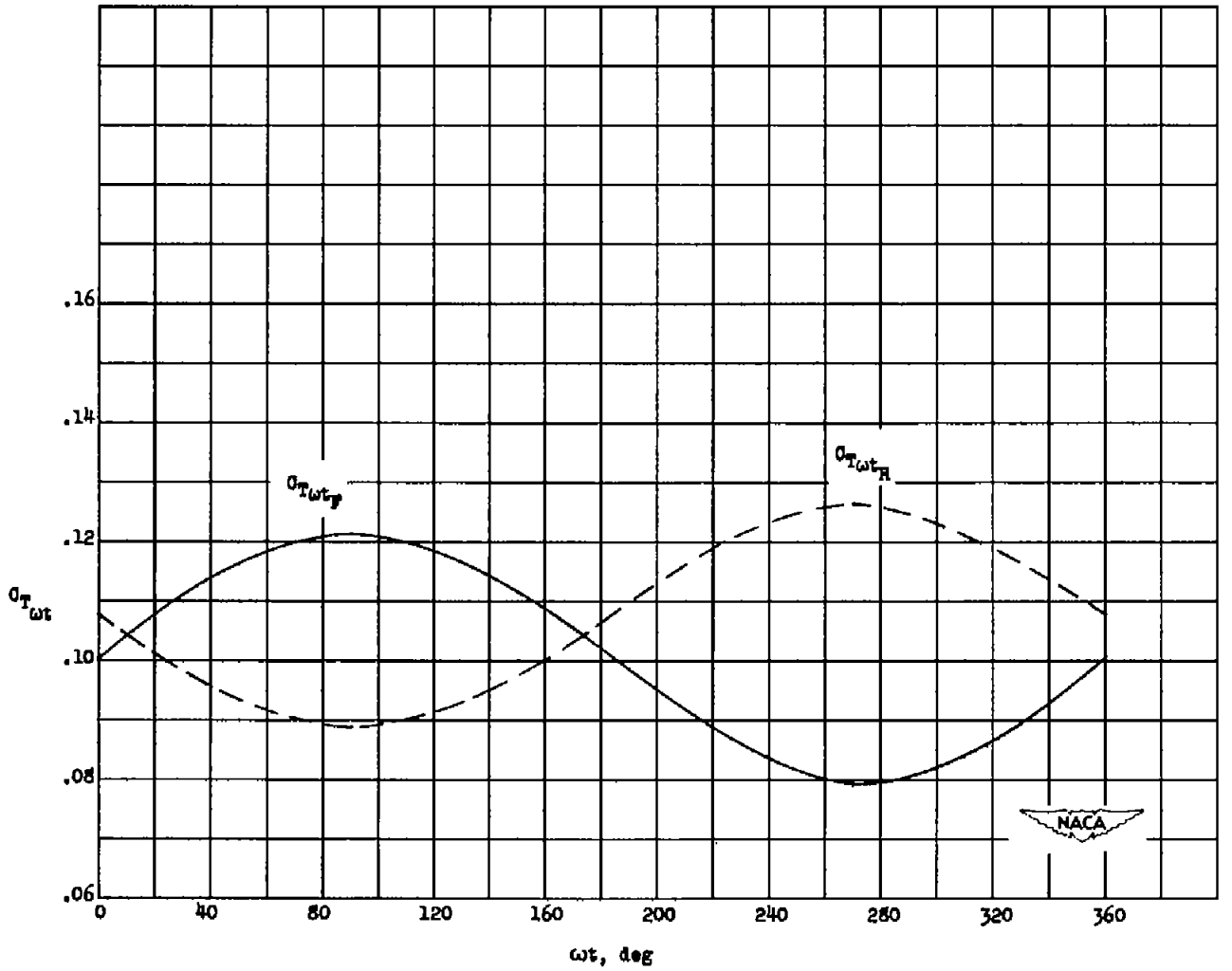

Figure 6.- Variation of instantaneous thrust coefficient $\left(C_{T_{\omega t}}\right)_{F,R}$ with blade position. M = 0.30; J = 1.20; $\alpha_T = 4^\circ$.

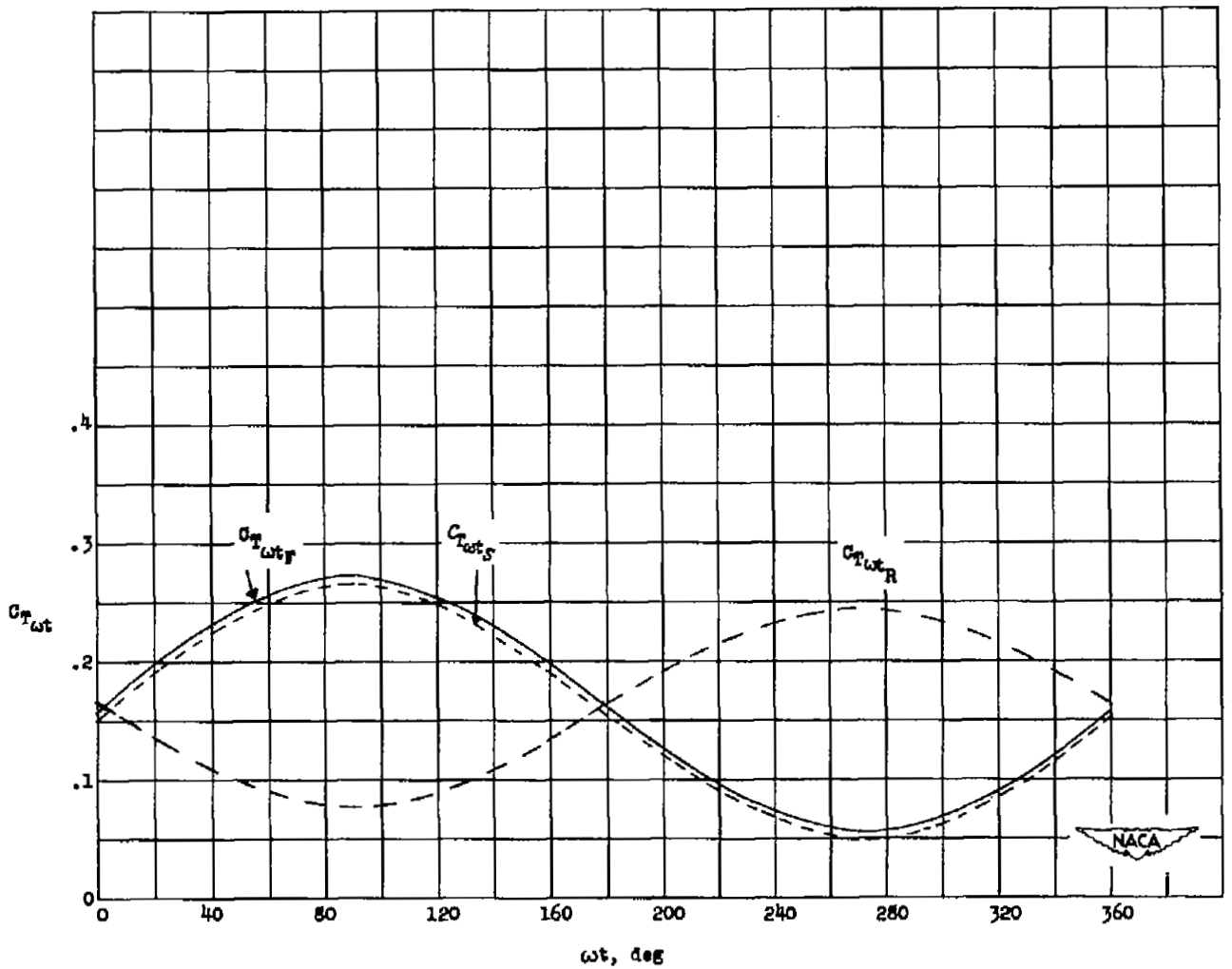

Figure 7.- Variation of instantaneous thrust coefficient $\left(C_{T_{\omega t}}\right)_{F,R}$ with blade position. $M = 0.623$; $J = 3.25$; $\alpha_T = 4^\circ$.

[redacted]